UNIVERSITY OF TARTU
Faculty of Science and Technology
Institute of Physics

Madis Kaspar Nigol

ESTCube-2 Attitude and Orbit Control System Sensor Selection and Temperature Calibration

Bachelor's thesis (12 ECTS)

Supervisors:
Dr. Andris Slavinskis
Hendrik Ehrpais

Tartu 2017

ESTCube-2 Attitude and Orbit Control System Sensor Selection and Temperature Calibration

Sensors based on micro-electro-mechanical systems are rising in popularity. These sensors are advancing in performance and dropping in price, which makes them suitable to use on nanosatellites. In the extreme conditions of space, the sensor's physical properties change and therefore sensors become inaccurate. This thesis is focused on calibrating gyroscopes, magnetometers and accelerometers on an existing prototype board. In this thesis, gyroscopes are tested in a thermal chamber while rotating the setup on a rotating bench. Accelerometers and magnetometers are tested in the thermal chamber at standstill. Furthermore, a suitable sensor is chosen from this selection for the ESTCube-2 nanosatellite.

Keywords: attitude determination, ESTCube-2, MEMS sensors, calibration, thermal chamber, CERCS T320 Space Technology

ESTCube-2 asendi ja orbiidi kontrollsüsteemi andurite valik ning temperatuurikalibratsioon

Mikroelektromehaanilistel süsteemidel põhinevad andurid koguvad aina populaarsust. Nende andurite sooritusvõime järjest paraneb, samas kui hind langeb, mis teeb need sobivaks kasutamiseks nanosatelliitidel. Kosmose ekstreemsetes tingimustes nende andurite füüsilised omadused muutuvad ning seetõttu muutuvad andurid ebatäpseteks. Käesolev töö keskendub olemas oleva asendi ja orbiidi kontrollsüsteemi prototüüpplaadil olevate güroskoopide, magnetomeetrite ja kiirendusandurite kalibreerimisele. Güroskoobid testitakse termokambris samaaegselt neid pöörates, kasutades pöördpinki. Magnetomeetrid ja kiirendusandurid testitakse termokambris paigalseisus. Lisaks valitakse nende andurite hulgast sobivaimad, mis lähevad ESTCube-2 nanosatelliidi pardale.

Märksõnad: asendi määramine, ESTCube-2, MEMS andurid, kalibratsioon, termokamber CERCS T320 Kosmosetehnoloogia

Contents

Acronyms

ADCS	Attitude Determination and Control System
AOCS	Attitude and Orbit Control System
CMOS	Complementary metal-oxide-semiconductor
COTS	Commercial off-the-shelf
E-sail	Electric Solar Wind Sail
FPGA	Field-programmable gate array
HAL	Hardware Abstraction Layer
HPF	High Pass Filter
LEO	Low Earth Orbit
LPF	Low Pass Filter
MCU	Microcontroller Unit
MEMS	Micro-Electro-Mechanical Systems
RMS	Root mean square
RTOS	Real-Time Operating System
SPI	Serial Peripheral Interface
UART	Universal Asynchronous Receiver/Transmitter
UKF	Unscented Kalman Filter
USB	Universal Serial Bus

Introduction

ESTCube-2 is a 3-unit nanosatellite developed by the Estonian Student Satellite Foundation. The satellite's main mission is to conduct a plasma brake experiment using Coulomb drag effect. If this experiment is a success, Coulomb drag propulsion technology can be used to deorbit spacecraft which have reached the end of their lifespan [1]. This is necessary to clean Earth's orbits, which are filling up at an increasing rate [2]. In addition to the main payload, there are multiple secondary payloads. The optical payload consists of two Earth observation imagers that measure a narrow spectral band for monitoring vegetation. High speed communication payload developed by Ventspils University that aims to have minimal data-rate of 1 Mbps. Corrosion resistant coating that will be tested to be able to protect spacecraft from atomic oxygen.

For the mission to be successful, the satellite needs an Attitude and Orbit Control System (AOCS). AOCS first takes care of the detumbling process after getting ejected from a carrier rocket. Then it is responsible for determining where the satellite is pointing by measuring it with sensors, running gathered data through algorithms such as unscented Kalman filters or light unscented particle filters. The processed data can then be used to run the control algorithms and operate the actuators that point the satellite in the required direction.

The aforementioned sensors have output dependent on various environmental conditions. In space, the main conditions to take into account are temperature and vacuum. Temperature change creates bias on the sensor, which needs to be corrected, leading to the aim of this work, which is to perform thermal calibration of AOCS gyroscopes, magnetometers and accelerometers. On gyroscopes, the calibration is performed at different rotational speeds as the gyroscope gain is also dependent on the rotational speed itself. In addition to calibration, these sensors are also compared to each other to select the most suitable, which will go on the ESTCube-2 satellite.

Chapter 1

Overview

1.1 ESTCube-2 and ESTCube-3 Missions

The main mission of ESTCube-2 is to further test a plasma brake using the Coulomb drag propulsion technology. The technology was also tested on ESTCube-1 (but did not work due to suspected mechanical breakdown of the payload motor) [3] and is planned to be tested on Finnish nanosatellite Aalto-1 [4]. Additional payloads include an Earth observation camera, high speed communication module and a corrosion resistant coating experiment. [5] [6]

ESTCube-2 will be sent to a Low Earth Orbit (LEO) at 600-700 km. For the plasma brake experiment, a 300 m tether is deployed using cold gas thrusters and reaction wheels or magnetic torquers. Magnetic torquers are added on ESTCube-2 for additional angular momentum generation as the cold gas thrusters only have enough fuel to extend 50 m of tether. However, outside of the magnetic field (for example on Lunar Orbit), the magnetorquers have no use.

ESTCube-3 will be based on ESTCube-2 with the primary mission to measure the Electric Solar Wind Sail (E-Sail) force in solar wind condition. ESTCube-3 will be sent on a lunar orbit or a highly elliptical Earth orbit to avoid Earth's magnetic field because it blocks the solar wind that would propel the spacecraft.

1.2 Overview of ESTCube-2 Attitude and Orbit Control System

The AOCS on ESTCube-2 is developed using the lessons learned from ESTCube-1. It has gyroscopes, magnetometers, accelerometers, sun sensors, and a star tracker to acquire data.

Raw data acquired from sensors must be processed to minimize noise and improve accuracy. On ESTCube-1, an Unscented Kalman Filter (UKF) was used. ESTCube-2 is testing a novel algorithm called Light Unscented Particle Filter, that is based on UKF and other particle filters, as the main attitude determination algorithm. The algorithms are tested and evaluated in a simulation environment built in Matlab and Simulink. Magnetorquers, which are developed in-house, cold gas thrusters and reaction wheels are used for attitude control. [7]

To unreel the E-sail tether on ESTCube-2 the AOCS has to spin the satellite around the same axis the tether reel is in. That can be started using cold gas thrusters and continued with the magnetorquers. For the optical payload, the satellite needs to point at a fixed place. That requires accuracy of 0.25° while the stability needs to stay between ± 0.125 deg/s.

1.3 AOCS Prototype Board

In 2014, Georgi Olentšenko developed a prototype board for AOCS. The board has an STM32F4 series ARM Cortex-M4 MCU, which is running at 84 MHz. Different sensors needed by AOCS have been placed on the board, including magnetometers, gyroscopes and accelerometers. The prototype board also has different connectivity options through pinheaders. [8] The MCU is running FreeRTOS, which it uses to manage processes, including reading data from the sensors. Most of the software for the board has been written previously and uses the STM32 Hardware Abstraction Layer (HAL). This board is used to perform tests on the sensors.

1.4 Thesis objectives

The objectives of this thesis are to:

- acquire or make the testing equipment for the sensors,
- write the missing drivers and fix the existing ones on the prototype board,
- figure out calibration methods, which will be used to characterize and calibrate the sensors,
- select the most suitable sensors from this prototype board, which will go on board of ESTCube-2.

Chapter 2

Sensors

2.1 MEMS technology

Micro-electro-mechanical systems (MEMS) is a technology in which electrical and mechanical parts are reduced to micrometre scale. This technology is used to make a variety of sensors and actuators. The size of MEMS devices enables to miniaturize products where sensors and actuators are used. An example is the rising popularity of nanosatellites in space technology.
In the design of small satellites, which are developed by students or small companies, both size and cost are important factors. In the last years, companies have brought many Commercial Off-the-Shelf (COTS) MEMS devices on the market. These devices are exceptionally precise, often surpassing their macroscopic counterparts, and bulk production has reduced the cost. These factors make MEMS devices perfect for use on a nanosatellite. [9] [10]

2.2 Sensors in AOCS

As COTS MEMS sensors have gained popularity and dropped in price, they will be used on ESTCube-2 AOCS. Sun sensors are used to track the position of the Sun relative to the spacecraft. For ESTCube-2, Hamamatsu s9226-04 [11] image sensors are used. The necessary electronics and the body of the Sun sensor will be developed in-house.

To track more distant stars than the Sun, a simple linear image sensor will not suffice. Instead, a star tracker is used. This means using a two-dimensional image sensor and an optics system. This system takes a picture of the stars and compares the picture to a database. When a match is found, it can be used to determine the spacecraft's attitude. This requires complicated and computation-heavy pattern matching algorithms. To cope with the computational need, an

FPGA (Field-programmable gate array) is used. As a dedicated unit, it allows great speed through heavy parallelization and does not occupy the main AOCS MCU resources.

The subjects of this thesis are gyroscopes, magnetometers and accelerometers. Gyroscopes measure the rotational speed, accelerometers measure acceleration and magnetometers measure the magnetic field. On ESTCube-2, magnetometers and gyroscopes are used to determine attitude, accelerometers are used for testing the cold gas thrusters. The magnetometer and gyroscope measurements are fed into the particle filter alongside with data from other sensors and simulations and the filter outputs the satellite's attitude based on that combined data. [7]

2.3 Sensor selection

In this section, the selected sensors and their characteristics according to datasheets are shown.

2.3.1 Gyroscopes

Four gyroscopes were initially selected for testing: MAX21000 [12] , BMG160 [13] , MPU-6000 [14] and L3GD20H [15] (Table 2.1). These gyroscopes were chosen because of their low noise (0.005 to 0.014 $\frac{\text{deg/s}}{\sqrt{\text{Hz}}}$), high resolution (16 bits, $0.001 - 0.011$ deg/s), high output data rate (ODR) (maximum at least 700 Hz) and optimal range (up to $\pm$2000 deg/s). The MPU-6000 sensor also includes an accelerometer. The MAX21000 is no longer manufactured and therefore will not be tested.

Sensor	Range	Resolution	Noise density	Current	Voltage	Temp	Interface	ODR range
MAX21000	$\pm$31.25 to $\pm$2000	16 bits / 0.001 deg/s	0.009 $\frac{\text{deg/s}}{\sqrt{\text{Hz}}}$	5.4 mA	1.71 to 3.6 V	-40 to +85°C	SPI / I2C	4.95 Hz to 10 kHz
BMG160	$\pm$125 to $\pm$2000	16 bits / 0.0038 deg/s	0.014 $\frac{\text{deg/s}}{\sqrt{\text{Hz}}}$	5 mA	2.4 to 3.6 V	-40 to +85°C	SPI / I2C	100 to 2000 Hz
MPU-6000	$\pm$250 to $\pm$2000	16 bits / 0.0076 deg/s	0.005 $\frac{\text{deg/s}}{\sqrt{\text{Hz}}}$	3.6 mA	2.375 to 3.46 V	-40 to +85°C	SPI / I2C	4 to 1000 Hz
L3GD20H	$\pm$250 to $\pm$2000	16 bits / 0.011 deg/s	0.005 $\frac{\text{deg/s}}{\sqrt{\text{Hz}}}$	5 mA	2.2 to 3.6 V	-40 to +85°C	SPI / I2C	11.9 to 757.6 Hz

Table 2.1: Selection of gyroscopes.

2.3.2 Accelerometers

Three accelerometers were chosen, from which two are 2-in-1 sensors with magnetometers (LSM303D [16] and FXOS8700CQ [17]) and one is a 2-in-1 sensor with gyroscope(MPU-6000), see Table 2.2. These accelerometers were chosen because of their high resolution (16 bits / 61 µg and 14 bits / 244 µg) and high ODR (800 Hz and 1600 Hz). In this thesis, unit g stands for gravitational acceleration not for gram.

Sensor	Range	Resolution	Noise density	Current	Voltage	Temp	Interface	ODR range
LSM303D	±2 to ±16 g	16 bits / 61 µg	150 $\frac{\mu g}{\sqrt{Hz}}$	300 µA	2.16 to 3.6 V	-40 to +85°C	SPI / I2C	3.125 to 1600 Hz
FXOS8700CQ	±2 to ±16 g	14 bits / 244 µg	126 $\frac{\mu g}{\sqrt{Hz}}$	240 µA	1.95 to 3.6 V	-40 to +85°C	SPI / I2C	1.563 to 800 Hz
MPU-6000	±2 to ±16 g	16 bits / 61 µg	400 $\frac{\mu g}{\sqrt{Hz}}$	3.6 mA	2.375 to 3.46 V	-40 to +85°C	SPI / I2C	4 to 1000 Hz

Table 2.2: Selection of accelerometers.

2.3.3 Magnetometers

Three magnetometers were selected for testing of which two are 2-in-1 sensors with accelerometers (FXOS8700CQ, LSM303D) and one is only a magnetometer (LIS3MDL [18]), see Table 2.3. These sensors were chosen because of their low noise (0.32 to 0.6 µT root mean square (RMS)), high resolution (6.1 to 36 nT) and high ODR (100 to 1000 Hz).

Sensor	Range	Resolution	Noise (RMS)	Current	Voltage	Temp	Interface	ODR range
LIS3MDL	±400 to ±1600 µT	16 bits / 14.6 nT	0.32 to 0.41 µT	270 µA	1.9 to 3.6 V	-40 to +85°C	SPI / I2C	0.625 to 1000 Hz
LSM303D	±400 to ±1200 µT	16 bits / 8 nT	0.5 µT	300 µA	2.16 to 3.6 V	-40 to +85°C	SPI / I2C	3.125 to 100 Hz
FXOS8700CQ	±1200 µT	16 bits / 100 nT	0.3 µT to 1.5 µT	240 µA	1.95 to 3.6 V	-40 to +85°C	SPI / I2C	1.563 to 800 Hz

Table 2.3: Selection of magnetometers.

2.4 Software development

The software developed for this work consists of multiple parts.

Embedded software

First, and the most important, part is the software on the prototype board. This software is written in C. Build and deployment are automated with GNU make and gcc 6.3.0. As the very base, the prototype board software has STM32 HAL. This HAL has been tweaked in some places and much has been added to it but STM32 original HAL still makes the majority part of the underlying software. An operating system called FreeRTOS is running on the MCU. Although it is not critically needed for this thesis, the main structure had already been made using this operating system and there was no need to remove it from the code.

To communicate with the on-board sensors drivers have to be used. Drivers are software libraries including functions to handle the initialization and communication of the sensors. As there are no readily usable libraries for this specific setup, previous students who worked on this board have written most of the necessary drivers.

When starting work on this board, it turned out that all but one driver worked, but the others read anomalous, incorrect data. Through months of studying C language and the legacy code, an understanding of the code was finally developed. In Februrary, logic analyzer was used, which could be hooked up to the Serial Peripheral Interface (SPI) lines and used to see the actual data moving over the lines.

Other tool for debugging was GNU Debugger (Gdb). With Gdb, the code can be run live, step-by-step, on the MCU, breakpoints can be inserted and variables printed where needed. Using these tools, the problem was found to be in the SPI protocol. Wrong mode of SPI was used during the communication and the reason that one driver worked, was that this driver used the exact mode by chance. This problem spread to all the drivers because the code was done in a copy-paste method without closer inspection. After fixing the SPI mode, all the sensors started working properly.

The next task was to implement the moving average method in C code. This had only few problems, main one being the initialization of the buffer. When initializing the buffer in C, it is unwise to fill the buffer with zeros because the longer the buffer, the greater effect on the results it will have. Therefore there is a longer time where the measurement is offset towards zero. Instead, it is reasonable to fill the buffer with real measurements first, because in that case, the buffer does not bias the outcome in the beginning.

Sensor data processing

There was a need to get all this data to the computer. As the communication was serial using Universal Asynchronous Receiver/Transmitter (UART), it made sense to connect to a communication port with hTerm (a terminal program to interact with serial devices). This program was also used in embedded software development and debugging phase. For few tests, hTerm was used to receive data and later saved to a .csv file to get it ready for processing. A Python script was written to set the speeds on the rotating bench (more on it in section 3.2), collect data and save it to correctly named files. Later on, a new script was made to collect all the data for the moving average tests. Making the tests automated saved time in the long run and these scripts can be used to make retests where needed.

After the data was received and saved in .csv files, it needed to be processed. For that, Matlab was used. It was reasonable to learn Matlab because it is a powerful tool for data analysis. First, a script was made for importing the data and extracting the data into variables. Secondly, these variables had to be plotted and the graphs exported into image files. After joining these two parts, a script to import data, extract it, make graphs and export them was completed.

Chapter 3

Testing methods and general setup

3.1 Physical setup

The requirement for the board was to be wireless because the board had to be fully rotatable. Otherwise, it is not possible to use the rotating bench (more on it in Section 3.2) as the wires would tangle and cause random movements of the board which would interrupt the sensor readings. The main parts to redesign were the power supply and the communication method. A single mini-USB (Universal Serial Bus) was used earlier for both data and power lines. J-Link, a debug probe for MCUs, which was used to flash the MCU and for debugging, could just be removed after flashing. When removing J-link SWD connector, the wires have to be removed while holding the reset button, otherwise the MCU will corrupt and will need to be reflashed.

To make the system wireless, the first thing to investigate was the power supply. A USB battery bank was used, which could be plugged into the mini-USB connector on the prototype board and could be charged with a micro-USB phone charger.

The second problem to tackle was communication. It was reasonable to still use UART and send data live instead of collecting it on a separate on-board device like SD card or FRAM. However, instead of a cable, it had to communicate via radio waves. There are devices called Serial-to-Bluetooth modules, which connect to receive and transmit wires and make a communication port accessible for the Bluetooth device connected to it. A module named HC-06 was used at a baud rate of 115.2 kbps. It could be connected to UART2 pins on the prototype board which were brought out on a separate pinheader. No code had been written to initialize this second UART channel, so the required initialization code was added for that. Later on, it was discovered that no code had also been written for the receiving part of the on-board UART but that functionality was added.

3.2 Rotating bench

To test the gyroscope's characteristics properly, it has to be tested on different rotational velocities as offset and bias may change not only with temperature but also with speed. In this thesis, only low speeds were tested because higher speeds needs construction of additional equipment, which was not feasible in the given timeframe. To achieve good accuracy of the bench, a stepper motor is used. For low speeds (0.1 - 3 deg/s), stepper motor can not be connected directly to the rotating board. The reason is that the stepper motor has a limited step size of 1.8° and if it was configured to low speeds, it would make small sudden steps resulting in non-consistent speed and heavy vibration.

To overcome this problem, a rotating bench using screw gear transmission has been made. At first, an existing stepper motor driver was used to rotate the bench. The speed was consistent but gyroscopes showed high noise, about 4 times bigger than gyroscope's noise density according to datasheets. This noise had two probable sources. First is the aforementioned limited step size. Every step, the stepper motor accelerates and decelerates, which means small changes in rotational velocity in gyroscope readings. This can be overcome using smaller microstepping than 1/2-full-step (which was the minimal microstep for the existing driver). The second noise contributor is the vibration of the bench itself. It has been shown that MEMS gyroscopes are sensitive to vibrations [19]. This can be improved by using dampening materials between the prototype board and the rotating bench.

After encountering and analyzing these problems, improvements had to be made. To reduce the vibrations, vibration dampening balls, which are similar to thick rubber washers, were put between the bench and the prototype board mount. For the microstepping, a new driver had to be made. An EasyDriver stepper motor driver was used, which allows for up to 1/8-microstepping. To control the driver, an Arduino Uno is used. Software for the Arduino was written using Arduino IDE and configured to receive commands, to control speed, over UART and set the EasyDriver to 1/8 Microstepping. The driver is powered with 9 V and consumes up to 750 mA [20].

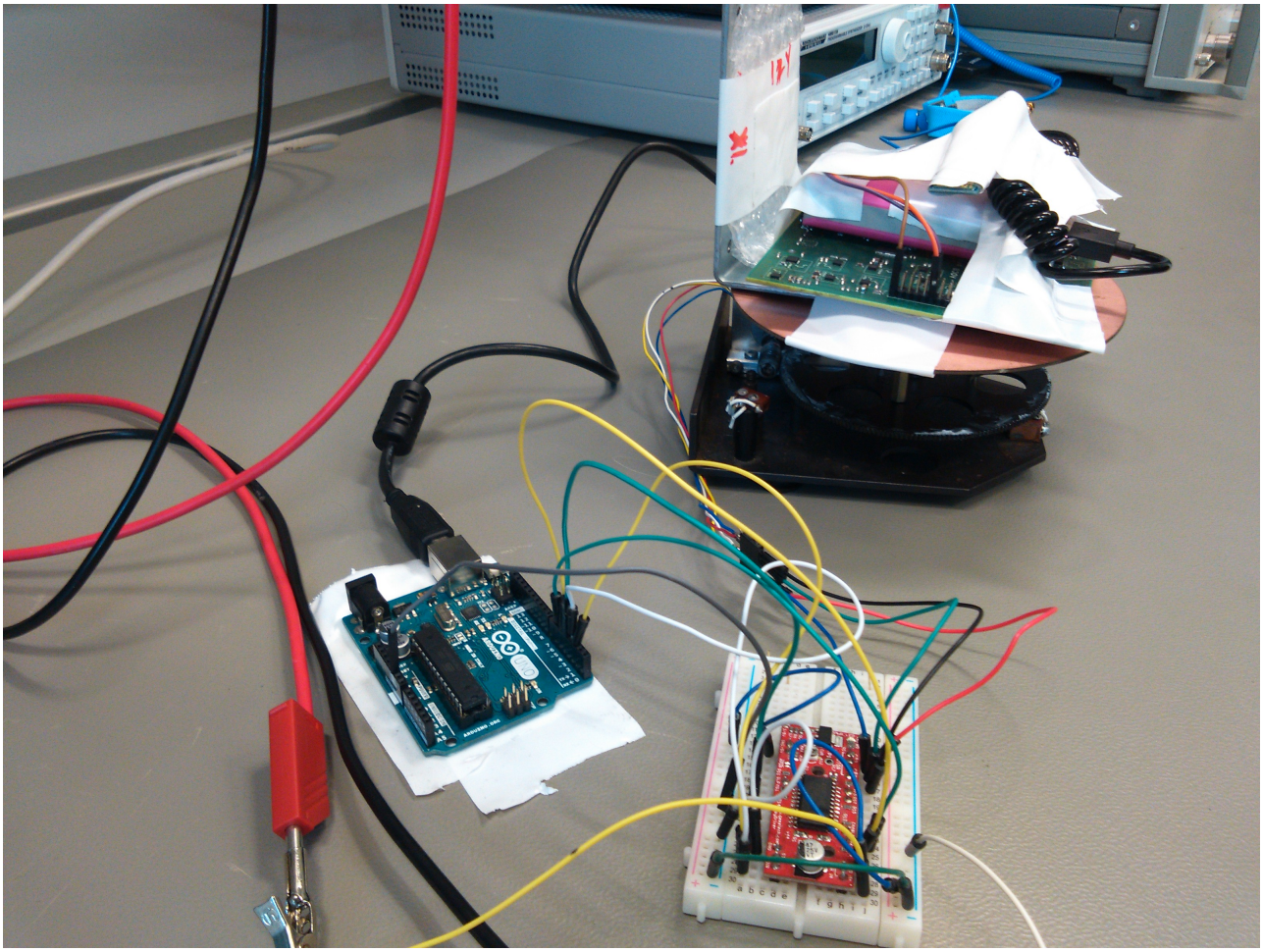

Figure 3.1: Test setup. From left to right: Arduino Uno, EasyDriver, rotating bench with the prototype board on top.

3.2.1 Rotating bench speed calculation

For conducting the tests, it is required to find the relation between the number inserted in the code and actual rotating bench speed. For that, time for one rotation with $n = 300$ and $n = 900$ were measured, where n is the parameter in the code. Five measurements were made with both speeds.

$n = 300$	$n = 900$	$n = 1200$
99.13 s	292.18 s	389.13 s
99.48 s	292.12 s	388.65 s
99.07 s	292.20 s	389.12 s
99.25 s	292.20 s	389.05 s
99.19 s	291.95 s	389.33 s

Table 3.1: Time for one rotation on different values of n.

From these, the average time for every value of n was taken — $t_{300} = 99.22$ s, $t_{900} = 292.13$ s and $t_{1200} = 389.06$ s. The goal was to get a function which takes rotational speed as an argument and outputs the value of n. To solve this problem, Mathcad 15 was used. Firstly, two matrices for speed and value of n were made.

$$v = \begin{bmatrix} \frac{360 \cdot \text{deg}}{t_{300}} \\ \frac{360 \cdot \text{deg}}{t_{900}} \\ \frac{360 \cdot \text{deg}}{t_{1200}} \end{bmatrix} \text{ and } n = \begin{bmatrix} 300 \\ 900 \\ 1200 \end{bmatrix}$$

Because the function appeared to be hyperbolic in nature, it was reasonable to linearize the inverse of the speed. Linear least squares method fitting of the equation $\frac{1}{v} = k \cdot n + b$ using Mathcad gave the result

$$f\left(\frac{1}{v}\right) = \frac{19.5154(\frac{1}{v} - 0.4088\text{s})}{\text{s}}, \tag{3.1}$$

where the speed is in units deg/s.

3.2.2 Rotating bench uncertainty

Type A uncertainty

Type A uncertainties can be found from measurements shown in Table 3.1. As the type A uncertainty, the mean value of standard deviations of time measurement at every n is used.

$$u_A = \frac{\text{stdev}(T_{n=300}) + \text{stdev}(T_{n=900}) + \text{stdev}(T_{n=1200})}{3} = 0.153 \text{ s} . \tag{3.2}$$

Type B uncertainty

Type B uncertainty sources are the stopwatch resolution and human reaction time. As human reaction time is not definable explicitly, it is presumed to be included in statistical uncertainty.

The stopwatch has resolution $\Delta = 0.01$ s. Therefore type B uncertainty is

$$u_A = \frac{\Delta}{\sqrt{3}} = 0.06 \text{ s} . \tag{3.3}$$

Combined uncertainty

Type C uncertainty is

$$u_C = \sqrt{u_A^2 + u_B^2} = 0.153 \text{ s} . \tag{3.4}$$

Therefore, speed uncertainty is

$$u_{speed} = \sqrt{\left(\frac{\mathrm{d}}{\mathrm{dt}} \frac{360 \cdot \text{deg}}{t} \cdot u_C\right)^2} = 0.006 \ \frac{\text{deg}}{\text{s}} . \tag{3.5}$$

Given confidence interval of 95.45%,with 4 degrees of freedom, the k-factor is 2.869. The extended uncertainty for speed is

$$u_{speed-extended} = 2.869 \cdot u_{speed} = 0.017 \ \frac{\text{deg}}{\text{s}} . \tag{3.6}$$

To get the uncertainty for n, the formula used was

$$u_n = \sqrt{\left(\frac{\mathrm{d}}{\mathrm{dt}} f(t) \cdot u_C\right)^2} = 0.48 , \tag{3.7}$$

where the function f (3.1) is in the shape

$$f\left(\frac{1}{\nu}\right) = \frac{19.5154(\frac{t}{2\pi} - 0.4088\text{s})}{\text{s}}, \tag{3.8}$$

The extended uncertainty for n is

$$u_{n-extended} = 2.869 \cdot 0.48 \approx 1.4 . \tag{3.9}$$

3.3 Moving average method

Sensor measurements tend to have a lot of noise. These noise sources include the characteristic noise density of the sensor as well as errors arising due to vibrations and from the test equipment itself. Using completely raw data is very inaccurate but there are ways to fight this noise. The most low-level methods are embedded within the sensors themselves as most MEMS sensors include some sort of noise cancellation methods. The most common method is a low pass filter (LPF), which only lets through signals at frequencies lower than the set cut-off frequency. Another one is the opposite of LPF — a high pass filter (HPF), which lets through signals with frequencies above the cut-off frequency.

There are also methods to eliminate noise on a higher level. The simplest method is to average over N samples. However, this technique means that N times fewer output values are received. To bypass this loss in output frequency, there exists a method called moving average. This method uses a FIFO (first in, first out) type buffer to average over N samples but to do so on every taken measurement. In this buffer, last N measurements are stored and simple averaging is performed on this buffer at every step. At each step, the earliest measurement in the buffer is removed and the latest measurement is inserted in the end. In code, it can be implemented by the following algorithm:

- Define an array with length N, where N is the length of the buffer
- Define an integer holding the sum of the elements in this array
- On every iteration of a loop reading the sensor data do the following:
  - Read data
  - Update the sum by $Sum = Sum - earliestMeasurement + currentMeasurement$
  - Output Sum/N
  - Shift the buffer left by 1
  - Insert the latest measurement in the end of the buffer.

The question when using a moving average is the length of the buffer. Smaller buffer means more noise but also rapid response to sudden changes in the signal. The longer the buffer, the smoother the signal is. Sudden changes in the signal are flattened down by the averaging over the length of the buffer. On an MCU, the memory is very limited, so from that perspective, smaller buffer is better. The Kalman filter, on the other hand, benefits from as low noise as possible in its input.

To solve this problem, a for-loop around the implemented moving average was added, which will go through N sizes ranging from 1 to 100. On sensors, at every N, 2000 samples were taken. Before starting to take the actual samples, at every N, 100 dummy measurements were taken to fill out the buffer beforehand. The reason behind it is that due to sensor measurement offset, the standstill data coming from the measurements is not actually zero. For example, if the output is 60 but the initial buffer is filled with zeros, the output will initially rise from 0 to 60 which in turn increases the standard deviation unnecessarily.

After collecting the data using Matlab, the standard deviation of measurements was plotted at each N against the value of N. The standard deviation characterizes the sensor output noise.

3.4 Temperature measuring

A thermistor was used to measure temperature in the thermal chamber more accurately than the chamber itself can show. This thermistor's resistance was measured using a multimeter. The thermistor was placed on the prototype board and fixed with tape. The measurements for the AOCS sensors were taken when the temperature had stabilized to fluctuate under 0.5°C. During the course of measurements, the maximal and minimal resistances (temperatures) were recorded at a temperature stabilized to fluctuations under ± 0.5°C and the average was used as the plotted temperature. The thermistor was already calibrated and Steinhart-Hart coefficients found to compute the temperature from Steinhart-Hart equation [21].

Chapter 4

Testing and characterization of gyroscopes

4.1 Moving average tests

The tests for finding the optimal buffer length for the moving average were performed on gyroscopes.

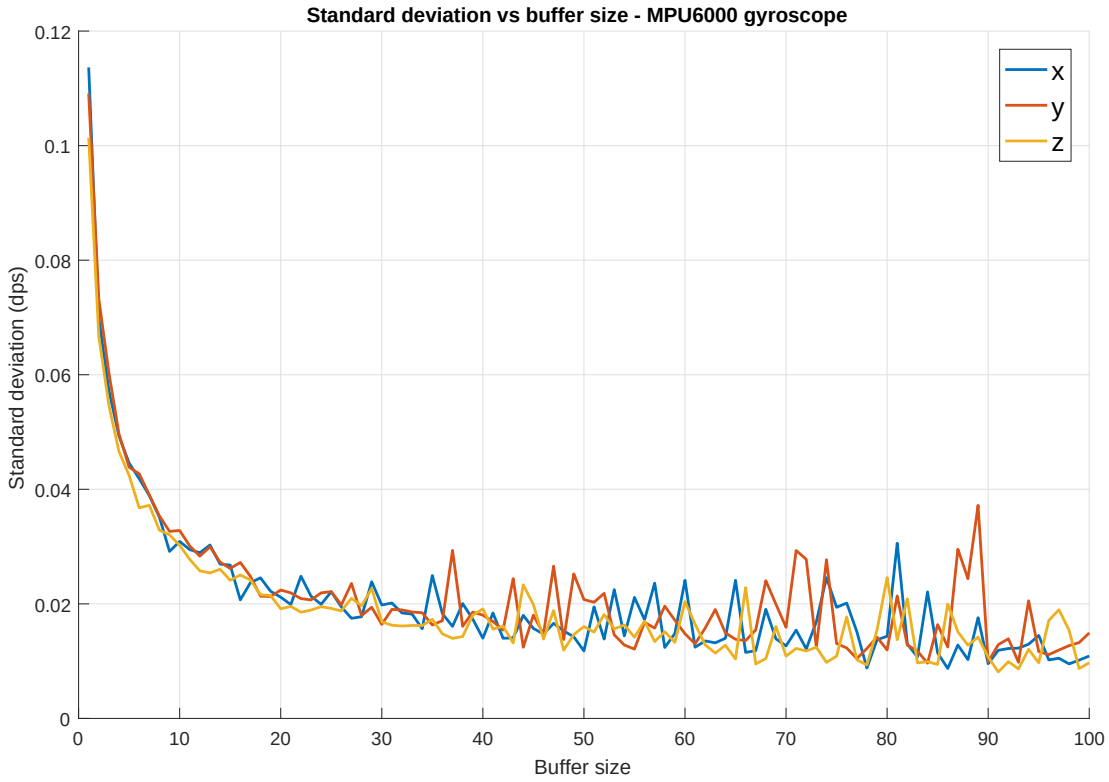

Figure 4.1: MPU-6000 gyroscope moving average test.

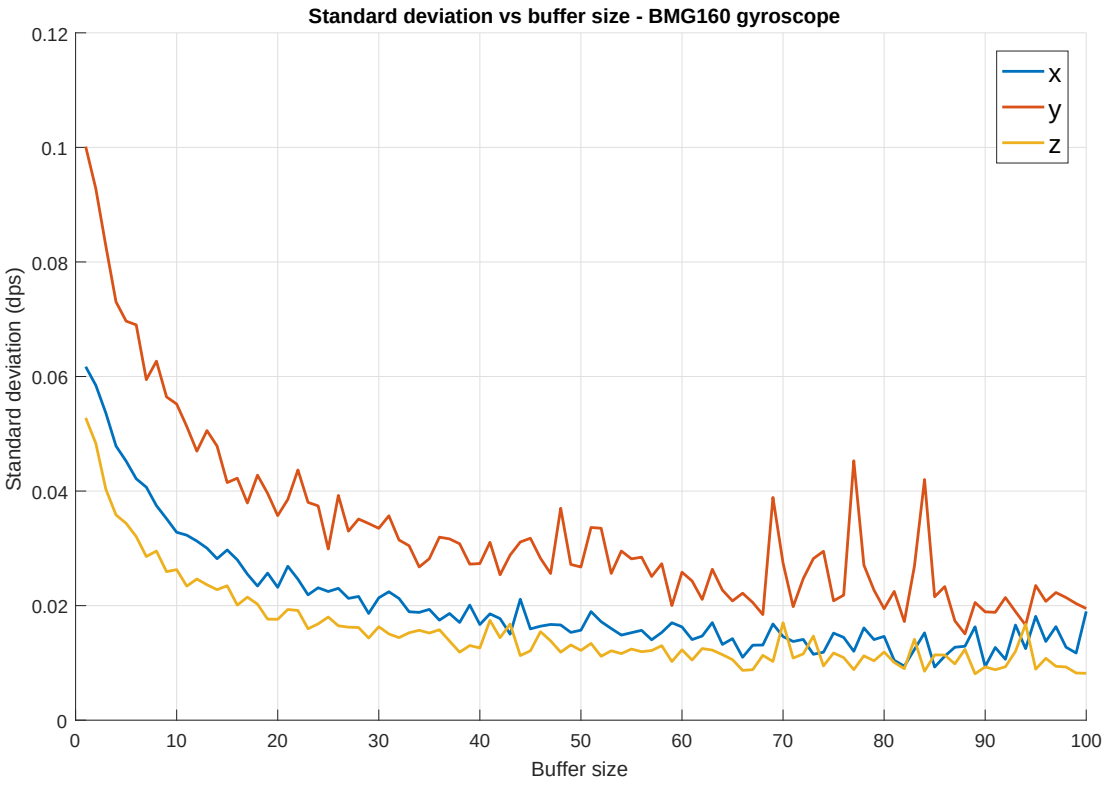

Figure 4.2: BMG160 gyroscope moving average test.

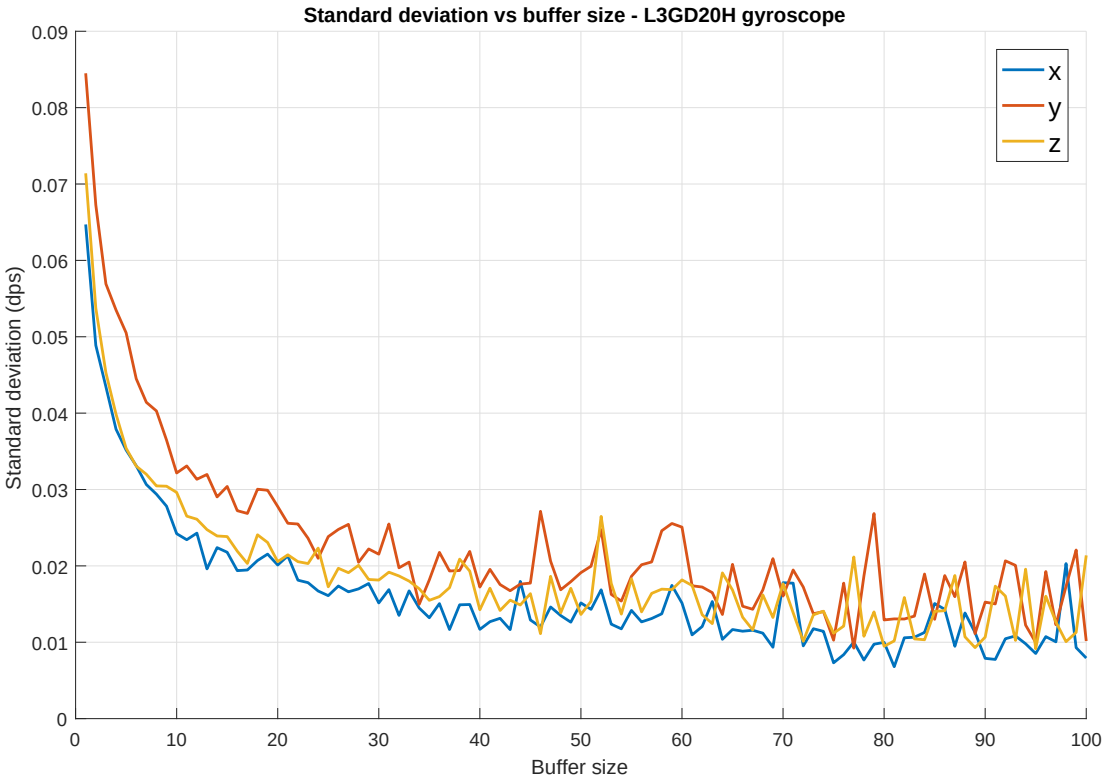

Figure 4.3: L3GD20H gyroscope moving average test.

From the graphs (see Figure 4.1, 4.2 and 4.3) it was decided that the optimal length of the buffer would be $N = 40$. The same buffer length was decided to be used on every gyroscope to keep the conditions similar.

4.2 Test setup

4.2.1 Gyroscope testing plan

Gyroscopes are tested on a rotating bench. Nine different speeds are chosen, the range of which is limited by the rotating bench — 0 deg/s, 0.1 deg/s, 0.2 deg/s, 0.5 deg/s, 0.7 deg/s, 1 deg/s, 2 deg/s, 2.5 deg/s and 3 deg/s. Although the range of speeds is small compared to gyroscope operating range, it is important because slow speeds have to be accurate during satellite pointing.

Normal conditions

Under normal conditions, meaning lab temperature of around 20°C, only the moving average buffer length tests (further in Section 3.3) are performed. There is no need to try that in different temperatures as the shape of the functions is important there, not the specific values.

Thermal chamber

In thermal chamber, four temperatures were chosen — -20°C, 0°C, 20 °C, 60 °C. These temperatures should give enough points to get adequate calibration functions. The limits -40°C and 80°C are not tested because of the risk of the board breaking. When a temperature is reached, it will have to stabilize until fluctuations are less than 0.5°C. At every temperature, 1000 samples at every speed on every gyroscope were collected to compromise for both speed of the tests and size of data.

4.2.2 Gyroscope configurations

The objective was to choose the most optimal and high performance settings for each sensor.

MPU-6000 gyroscope

- Sample rate 1 kHz
- Digital low pass filter with Bandwidth 5 Hz.
- Range $\pm$250 deg/s
- No sleep or low power mode enabled

BMG160 gyroscope

- Output data rate 100 Hz
- Data filter bandwidth 32 Hz.
- Range $\pm$125 deg/s
- No sleep or low power mode enabled

L3GD20H gyroscope

- Output data rate 100 Hz
- Cut-off frequency 12.5 Hz
- Range $\pm$250 deg/s
- No sleep or low power mode enabled

4.3 Thermal chamber tests

Gyroscopes were tested on a rotating bench in the thermal chamber with a moving average buffer of length 40. When the temperature had stabilized enough, a Python script was run, which collected 1000 samples from every gyroscope on 9 different speeds. The four different temperatures were -20.4°C, 0.1°C, 20.2°C and 59.8°C. Each temperature varied $\pm$0.2°C.

As the gyroscopes were tested in different rotating speed at different temperatures, the calibration was not straightforward. As the bias changes with both offset and temperature, the calibration functions needed to be multi-level. The final decision was to get two types of

calibration functions. Both functions have the shape of second order polynomial function

$$f(x) = p1 \cdot x^2 + p2 \cdot x + p3 \; . \tag{4.1}$$

The first type of function takes rotational speed as an argument and outputs a polynomial coefficient. These polynomial coefficients are used to get second-order polynomial functions. These functions are the second type of functions. As the speed is accounted for at this point, this function takes temperature as the argument and outputs the offset which needs to be added to the taken measurement.

For example, calibrating BMG160 z-axis. Let the rotating speed be 3 deg/s around the z-axis. In that case, first, the speed is put into the first type of function. There are 3 of these functions as the next function for temperature correction is a second-order polynomial function and therefore needs 3 polynomial coefficients. With gained coefficients, a new function can be formed, which corrects for temperature and is shown in Figure 4.3. On that figure, raw measurements at different temperatures (blue line), the polynomial function to calibrate for the temperature (red line) and the calibrated function (yellow line) are shown.

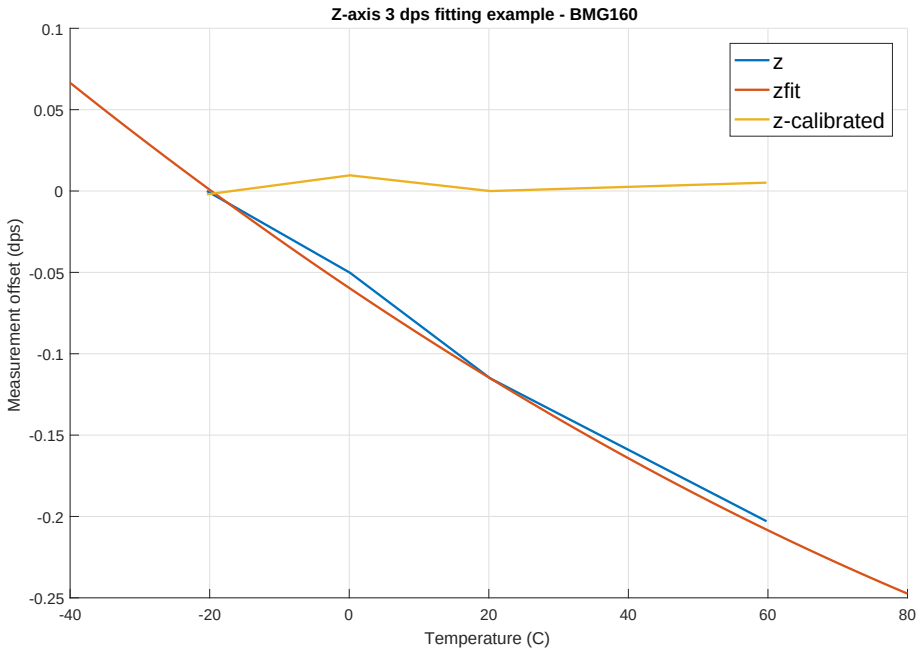

Figure 4.4: Example of a temperature calibration function on BMG160 z-axis at 3 deg/s.

By examining the raw data, a periodical noise was found in the axis the system was revolving around but at every speed, the noise had a different period. After further investigation, it seemed that the source for this was a small eccentricity in the screw gear which was rotating the main board. Due to this systematic error, only rotation around z-axis was done and the procedures for

calibration were developed from that data. To calibrate all axes correctly, this error needs to be eliminated and the rotating bench must support higher speeds and must have minimal vibration. Therefore, new tests will not be conducted before building a new testing bench.

The coefficient values for z-axis speed calibration functions which give the coefficients for temperature calibration functions are brought out in Table 4.1. These coefficients go in a polynomial function with the function 4.1.

Coefficients	p1-speed	p2-speed	p3-speed
p1-BMG	$2.072 \cdot 10^{-7}$	$-1.685 \cdot 10^{-7}$	$5.338 \cdot 10^{-6}$
p2-BMG	$-1.558 \cdot 10^{-5}$	$-2.785 \cdot 10^{-4}$	$-1.908 \cdot 10^{-3}$
p3-BMG	$-4.897 \cdot 10^{-4}$	$-5.144 \cdot 10^{-3}$	$-3.973 \cdot 10^{-2}$
p1-MPU	$7.840 \cdot 10^{-6}$	$-2.124 \cdot 10^{-5}$	$1.124 \cdot 10^{-4}$
p2-MPU	$-2.137 \cdot 10^{-4}$	$6.094 \cdot 10^{-4}$	$7.561 \cdot 10^{-3}$
p3-MPU	$-6.072 \cdot 10^{-3}$	$1.587 \cdot 10^{-2}$	$1.150 \cdot 10^{-1}$
p1-L3GD	$1.336 \cdot 10^{-6}$	$-1.197 \cdot 10^{-5}$	$-4.119 \cdot 10^{-4}$
p2-L3GD	$-3.755 \cdot 10^{-4}$	$1.747 \cdot 10^{-3}$	$-1.160 \cdot 10^{-1}$
p3-L3GD	$-7.381 \cdot 10^{-3}$	$3.534 \cdot 10^{-2}$	$-2.157 \cdot 10^{0}$

Table 4.1: Gyroscope z-axis calibration coefficients.

There was no consistent relation between standard deviation (STD) of measurements and temperature. The mean STDs are presented in Table 4.2.

Mean STD	x-axis (deg/s)	y-axis (deg/s)	z-axis (deg/s)
MPU-6000	0.064	0.057	0.051
BMG160	0.011	0.018	0.008
L3GD20H	0.020	0.024	0.025

Table 4.2: Mean standard deviations of gyroscope standstill measurements over temperature.

4.4 Uncertainty budget

The uncertainty components, from the tests and datasheets, of the gyroscope measurements are presented in Tables 4.3, 4.4, and 4.5. Normal distribution noise is assumed on all sensors.

Quantity	Uncertainty contribution in deg/s
Resolution	0.005
Sensitivity tolerance	0.03
Noise	0.06
Rotating bench	0.017
Total (RMS), 95.45% confidence level	0.14

Table 4.3: MPU-6000 uncertainty budget.

Quantity	Uncertainty contribution in deg/s
Resolution	0.0023
Sensitivity tolerance	0.01
Noise	0.015
Rotating bench	0.017
Total (RMS), 95.45% confidence level	0.05

Table 4.4: BMG160 uncertainty budget.

Quantity	Uncertainty contribution in deg/s
Resolution	0.005
Sensitivity tolerance	0.02
Noise	0.02
Rotating bench	0.017
Total (RMS), 95.45% confidence level	0.07

Table 4.5: L3GD20H uncertainty budget.

4.5 Final sensor selection

As MPU-6000 has much higher noise than BMG160 and L3GD20H, it was ruled out from the final selection. This might be due to different measurement frequencies and misconfiguration but that is to be confirmed. Although BMG160 and L3GD20H were quite similar in terms of noise with BMG160 being a bit better, the temperature offset is an order of magnitude higher for the L3GD20H than for the BMG160. Therefore, as the gyroscope for ESTCube-2, BMG160 is recommended.

Chapter 5

Testing and characterization of accelerometers

5.1 Moving average tests

The same procedure as on gyroscopes was performed on the accelerometers under normal conditions at standstill.

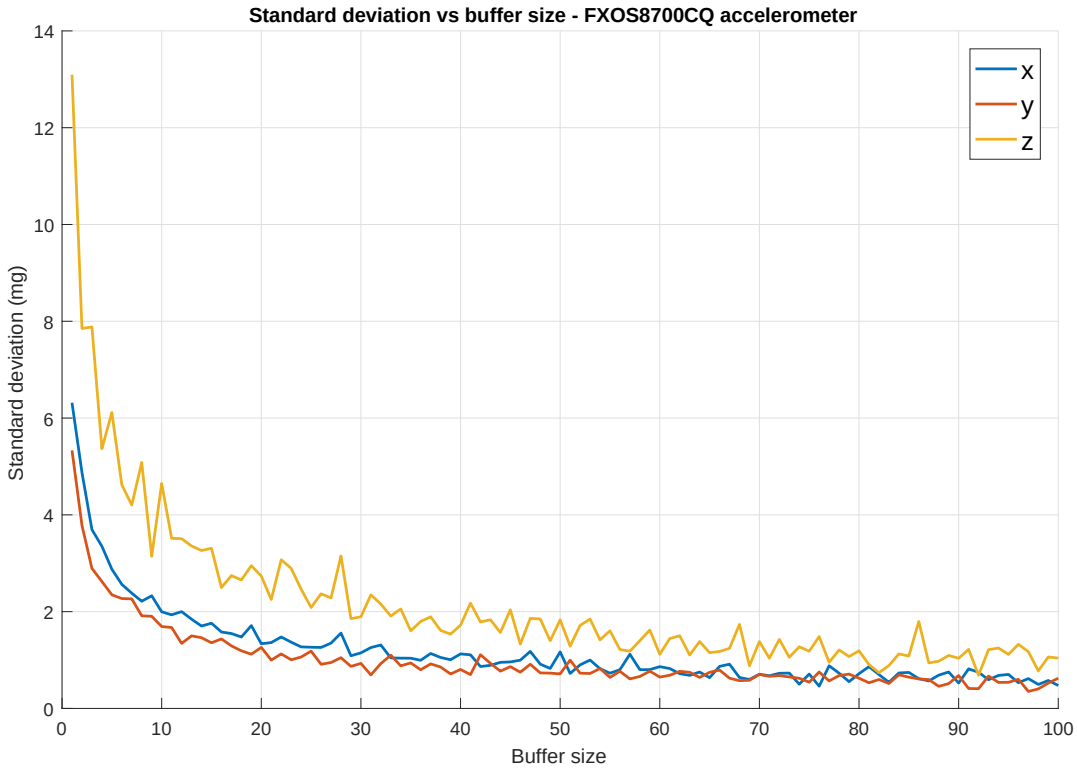

Figure 5.1: FXOS8700CQ accelerometer moving average test.

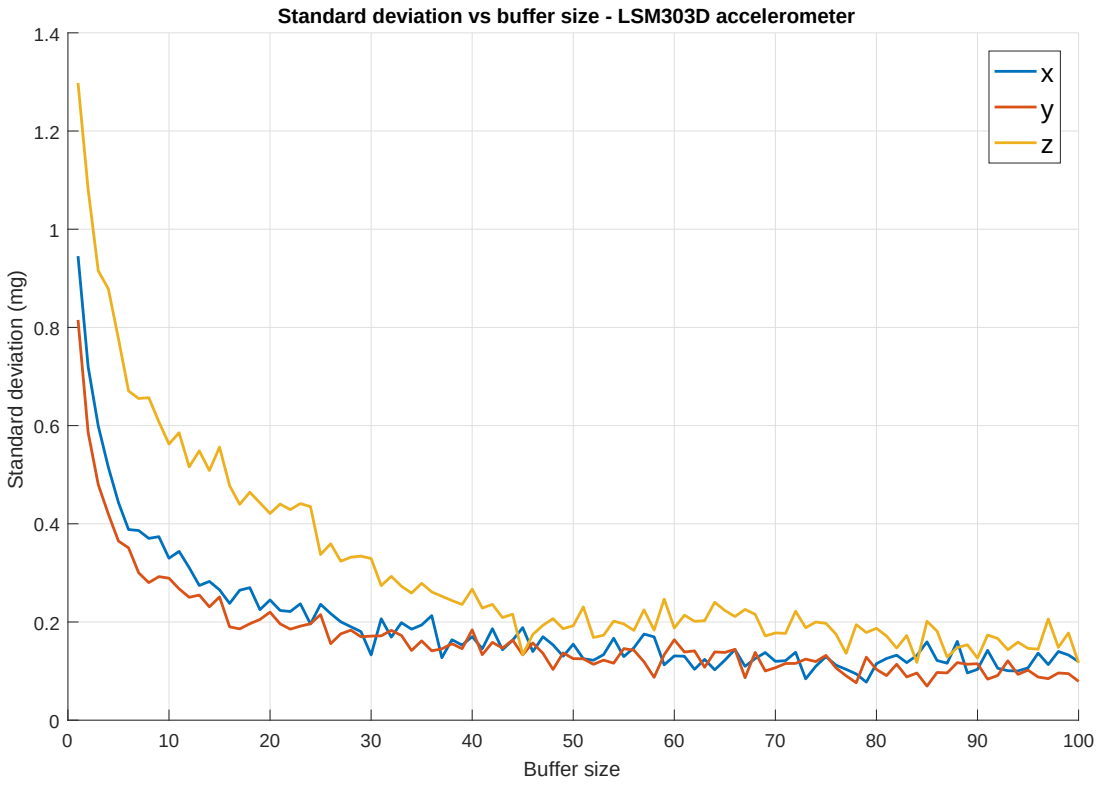

Figure 5.2: LSM303D accelerometer moving average test.

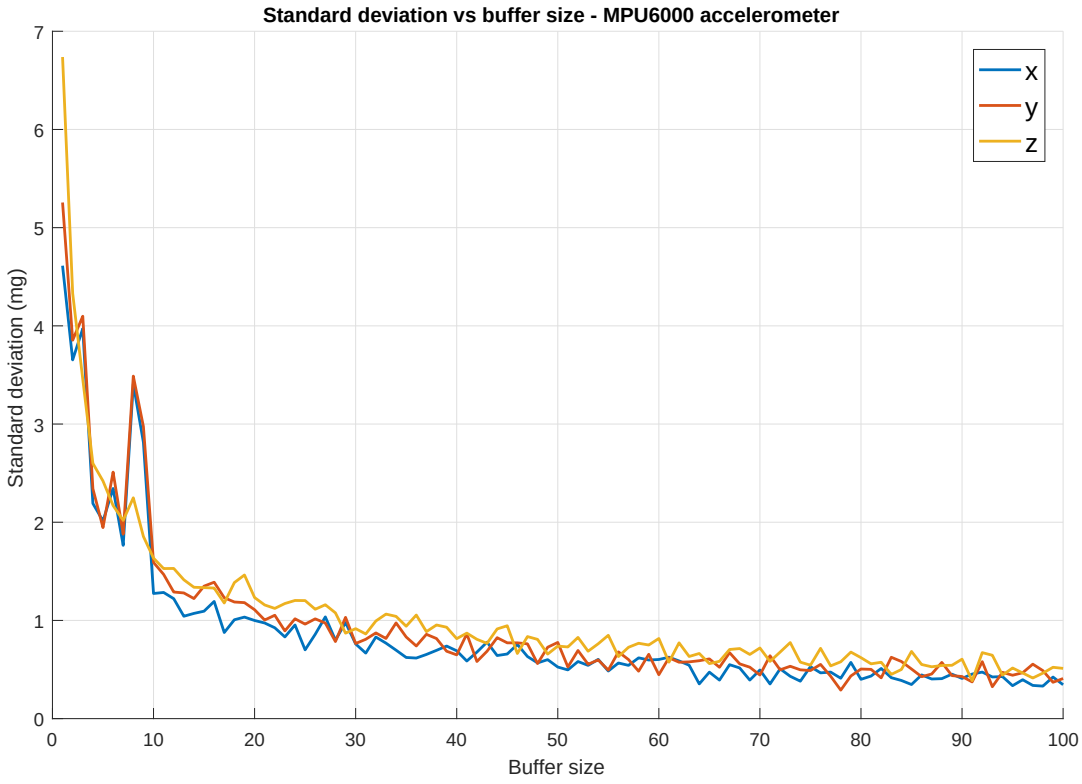

Figure 5.3: MPU-6000 accelerometer moving average test.

From these graphs (Figures 5.1, 5.2 and 5.3), I chose the moving average buffer length to be 40 (similar to gyroscopes) because there is no significant noise decrease after that and the response is faster with a shorter buffer.

5.2 Test setup

In this section, the testing plan for accelerometers is described and accelerometer configurations brought out for repeatability.

5.2.1 Accelerometer testing plan

In the scope of this thesis, accelerometers are tested only in standstill, measuring gravity. Further plans include testing accelerometers on a vibrating bench.

Normal conditions

Under normal conditions, only the moving average buffer length tests are performed.

Thermal chamber

In thermal chamber, four temperatures were chosen — -20°C, 0°C, 20 °C, 60 °C. When a temperature is reached, it will have to stabilize until fluctuations are less than 0.5°C. At every temperature, 1000 samples will be collected from each sensor.

5.2.2 Accelerometer configurations

FXOS8700CQ accelerometer

- Output data rate 25 Hz, hybrid mode
- Reduced noise mode enabled
- Range ± 2 g
- No sleep or low power mode enabled

LSM303D accelerometer

- Output data rate 100 Hz
- Anti-aliasing bandwidth 50 Hz
- Range ± 2 g
- No sleep or low power mode enabled

MPU-6000 accelerometer

- Output data rate 1 kHz
- Digital low pass filter with Bandwidth 5 Hz
- Range ± 2 g
- No sleep or low power mode enabled

5.3 Thermal chamber tests

The accelerometers were tested at a standstill inside the thermal chamber. It was running on the battery pack although it could have been supplied via power cable because the board was still. Moving average buffer length was set to 40. The measurements were taken at four temperatures: -19.6°C, 0.2°C, 20.4°C and 58.7°C. Each temperature varied ± 0.2°C.

The calibrated curves for temperature-inflicted offset were calculated for all axes and can be seen in Appendix A, Figures A.1, A.2, and A.3. From the graphs, it can be seen that FXOS8700CQ and MPU-6000 accelerometer got quite reasonable offsets and calibration polynomial functions. However, LSM303D has a flaw, where the accelerometer gets locked up to maximum values in brownouts (supply voltage drops below minimum operating level but not to zero). Initially, this flaw was bypassed through code by adding a delay in the initialization code between turning the power off and on, so that the voltage would drop completely during the reset. In thermal chamber tests however, this fix did not work. The accelerometer would lock up from temperatures -20 to 20°C. In 60°C it worked again. Instead of using an electronical hack on the board, it was decided that this sensor is not suitable for the ESTCube-2 because of its poor stability, which is especially critical in the space technology.

The standard deviations did not change in correlation with the temperature but randomly at each temperature. Retests are needed to confirm the lack of correlation. The mean standard

deviations are presented in Table 5.1.

Mean STD	x-axis (mg)	y-axis (mg)	z-axis (mg)
FXOS8700CQ	1.1	1.6	2.6
MPU-6000	0.8	1.1	1.8

Table 5.1: Mean standard deviations of gyroscope standstill measurements over temperature.

For the LSM303D, standard deviations are invalid because at first three temperatures, the standard deviations were zero as the accelerometer outputted constant value. Still, from the standard deviations of FXOS8700CQ and MPU-6000 it can be seen that the they are the biggest in the z-axis, which is the direction of Earth's gravity. Later, it should be tested if this observation holds for other axes as well when they are turned in the direction of gravity.

5.4 Uncertainty budget

The uncertainty components, from the tests and datasheets, of the accelerometer measurements are presented in Tables 5.2, 5.3, and 5.4. Normal distribution noise is assumed on all sensors.

Quantity	Uncertainty contribution in mg
Resolution	0.14
Noise	1.8
Total (RMS), 95.45% confidence level	3.6

Table 5.2: FXOS8700CQ uncertainty budget.

Quantity	Uncertainty contribution in mg
Resolution	0.035
Noise	0.25
Total (RMS), 95.45% confidence level	0.51

Table 5.3: LSM303D uncertainty budget.

Quantity	Uncertainty contribution in mg
Resolution	0.035
Noise	1.2
Total (RMS), 95.45% confidence level	2.4

Table 5.4: MPU-6000 uncertainty budget.

5.5 Final sensor selection

Initially the LSM303D seemed the most suitable sensor of the three. However, since the sensor showed unreliability, this sensor was not chosen. It depends on the requirements of the accelerometer accuracy if the MPU-6000 or FXOS8700CQ would also be suitable. As accelerometer data is not used in the attitude determination algorithms but instead for testing the cold gas thrusters, accelerometer may have more lax requirements, but that remains to be determined.

Chapter 6

Testing and characterization of magnetometers

6.1 Moving average tests

Initially, the same procedure, for determining the moving average buffer length, was also performed on magnetometers under normal conditions and at standstill. Later on, it became apparent that moving average can not be used on magnetometers on the satellite. The reason is that the magnetic field changes rapidly when the satellite is spinning. If the measurements were to be smoothened by averaging, then phase shift is introduced and due to that, old measurements are inputted into the particle filter and the wrong attitude determination received. These graphs (Figures 6.1, 6.2, and 6.3) are still shown in the thesis in case someone wants to use them for a purpose where moving average could be used on magnetometers (eg. a simple compass).

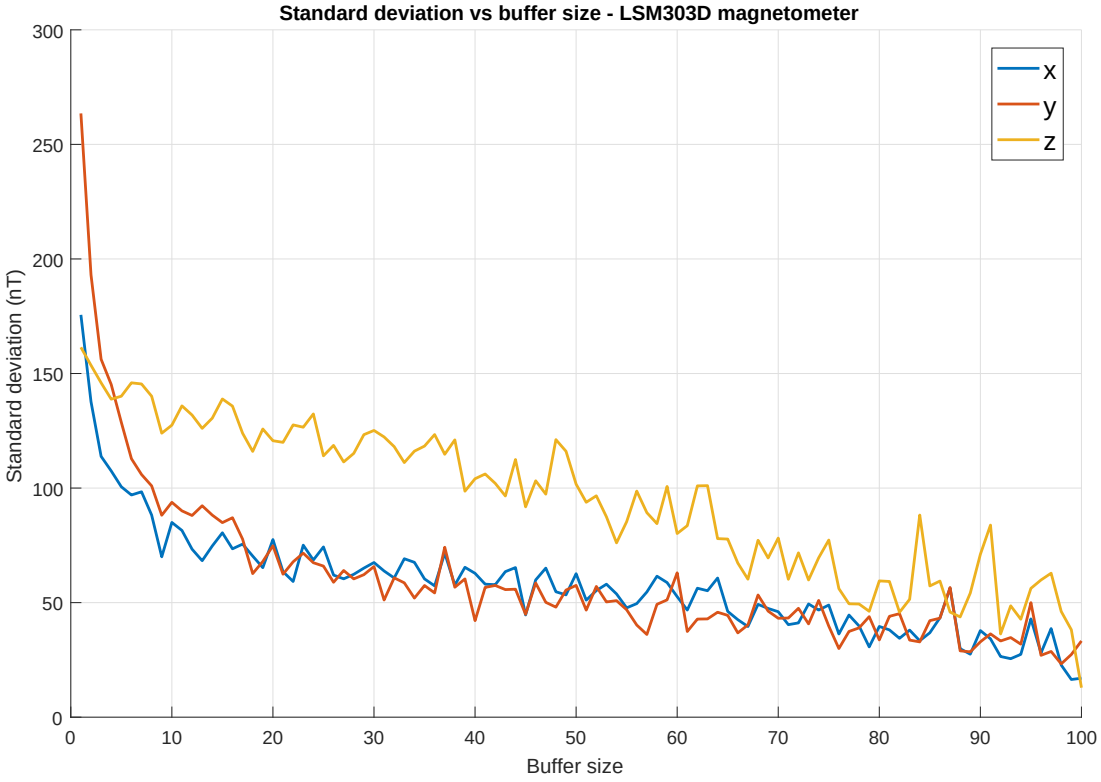

Figure 6.1: LSM303D magnetometer moving average test.

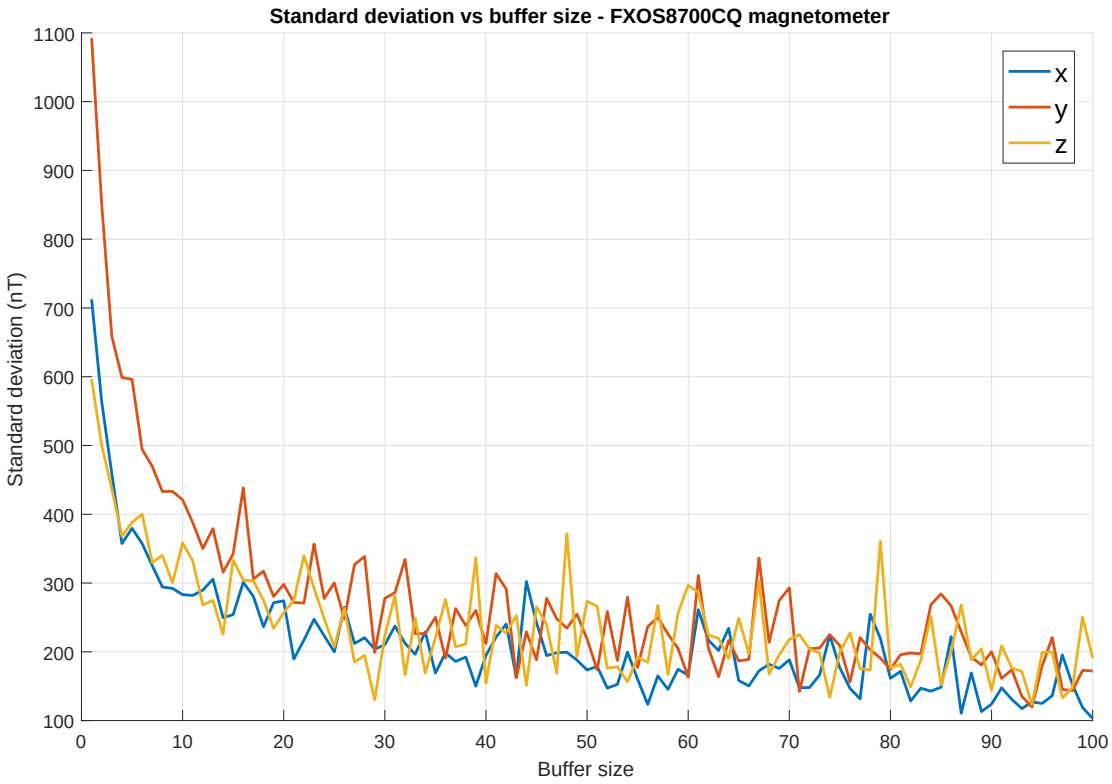

Figure 6.2: FXOS8700CQ magnetometer moving average test.

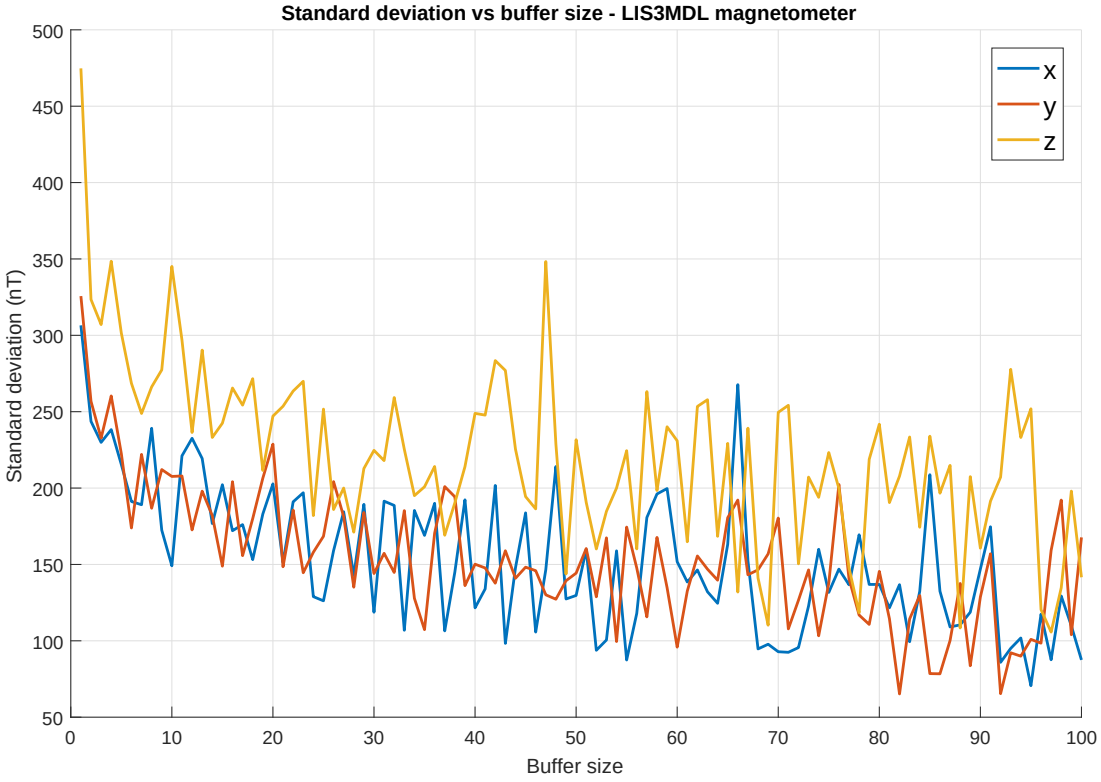

Figure 6.3: LIS3MDL magnetometer moving average test.

6.2 Test setup

In this section, the testing plan for magnetometers is described and magnetometer configurations are brought out to be able to repeat the experiments under same circumstances.

6.2.1 Magnetometer testing plan

In the scope of this thesis, magnetometers are tested only at standstill. Further plans include finishing the electronics and code for the Helmholtz coil, which is developed by members of ESTCube, and calibrating the sensors using that.

Normal conditions

Under normal conditions, only the moving average buffer length tests are performed.

Thermal chamber

In thermal chamber, four temperatures were chosen — -20°C, 0°C, 20 °C, 60 °C. When a temperature is reached, it will have to stabilize until fluctuations are less than 0.5°C. At every temperature, 1000 samples are collected from each sensor.

6.2.2 Magnetometer configurations

LSM303D magnetometer

- Output data rate 12.5 Hz
- Anti-aliasing bandwidth 50 Hz
- Range ±2 gauss
- No sleep or low power mode enabled

FXOS8700CQ magnetometer

- Output data rate 25 Hz, hybrid mode
- 32x oversampling
- Range ±12 gauss
- No sleep or low power mode enabled

LIS3MDL magnetometer

- Output data rate 20 Hz
- Ultra-high performance mode for all axes
- Range ±4 gauss
- No sleep or low power mode enabled

6.3 Thermal chamber tests

The magnetometers were tested at standstill in thermal chamber at four different temperatures. The board was supplied from a battery pack but could have been supplied externally instead. For the magnetometers, moving average buffer was removed and only raw data (with in-sensor filtering) was recorded. The temperatures where the measurements were taken: -18.9°C, 0.2°C, 20.0°C and 57.3°C. Each temperature varied $\pm$0.2°C.

The calibration curves for offset can be seen in appendix B, Figures B.1, B.2 and B.3. From the figures, it can be seen, that FXOS8700CQ and LIS3MDL magnetometers change in almost linear fashion with the temperature. LSM303D however, showed some erratic behaviour. As LSM303D did not show reliability as an accelerometer either, it could be discarded from the selection and is not worth of further testing.

The standard deviations seen on Figures B.4 and B.5 show less erratic behaviour than in accelerometers. FXOS8700CQ seemed to become noisier in higher temperatures with a drop at 20°C, which might be because the sensor had been optimized for normal conditions. LIS3MDL however, shows the opposite with small peaks at 20°C and sudden drop in noise at 60°C. To confirm this relation, more tests would have to be run.

6.4 Uncertainty budget

The uncertainty components, from the tests and datasheets, of the magnetometer measurements are presented in Tables 6.1, 6.2, and 6.3. Normal distribution noise is assumed on all sensors.

Quantity	Uncertainty contribution in μT
Resolution	0.008
Noise	1
Total (RMS), 95.45% confidence level	2

Table 6.1: LSM303D uncertainty budget.

Quantity	Uncertainty contribution in μT
Resolution	0.06
Noise	0.8
Total (RMS), 95.45% confidence level	1.6

Table 6.2: FXOS8700CQ uncertainty budget.

Quantity	Uncertainty contribution in μT
Resolution	0.009
Noise	0.9
Total (RMS), 95.45% confidence level	1.8

Table 6.3: LIS3MDL uncertainty budget.

6.5 Final sensor selection

Because of sensor unreliability, LSM303D is not suitable for the magnetometer either. This needs to be retested with a different chip as it is possible that the chip on-board is damaged. That leaves a choice between LIS3MDL and FXOS8700CQ. Although FXOS8700CQ showed lower noise, the difference was not significant enough and LIS3MDL is chosen for ESTCube-2. That is because LIS3MDL has more configurability and a smaller temperature offset. For example, FXOS8700CQ supports only one range but LIS3MDL has four different selectable ranges, which gives more flexibility.

Future work

As this is preliminary work for further calibration, most of the work is ahead. The main purpose of the thesis besides sensor selection and partial calibration was to learn about the techniques and difficulties of calibrating sensors. This purpose has been fulfilled as the author gained invaluable knowledge in that field which can be used to perform proper final calibration on all of the ESTCube-2 sensors.

As the rotating bench is flawed, a new system for rotational testing must be built. Preferably, it could be a 3-axis system with error less than 1°. This system also needs to be as vibration free as possible. After these problems have been eliminated, a new set of tests need to be conducted on gyroscopes at wider range of speeds.

Initial plan was to calibrate the magnetometers using the in-house built Helmholtz coil. Unfortunately, this coil's electronical side was not finished and due to time limitations, the electronics were not built as redesign was needed there. However, the Helmholtz coil will be finished and the magnetometers will be calibrated using that.

Accelerometers should be tested on a vibration bench as well. In this thesis they were only tested in standstill and in thermal chamber but to gain further insight about sensor behaviour, it needs to be exposed to different accelerations besides constant Earth gravitational acceleration.

All the sensors were tested for temperature change. However in space, important factor besides temperature is also vacuum. The sensors will be held in a vacuum chamber for a few days to see if there is any vacuum bias to be aware of.

Conclusions

Knowledge was gained about MEMS sensors and how to use them. The author got acquainted to thermal testing and has experience conducting experiments in the thermal chamber. Also experience was gained with mechanical errors and gained insight on how to avoid them. Sensor characterization and calibration methods were learnt and can be used to perform better calibration on ESTCube-2 sensors. During the work of this thesis, programming languages such as C, Python and Matlab were practiced.

For the thermal chamber tests, the temperature logging should have been done differently. Instead of recording the highest and lowest values during the test, the correct way would be to log temperature concurrently when taking measurements. This ensures more reliable data and that it can be statistically characterized. Ideally, all the sensors would have their own temperature sensors as well. In these tests, the temperature of the board was measured.

The moving average method for accelerometers and gyroscopes was used to lower the sensor noise and the noise from the rotating bench. The noise sourcing from the rotating bench was also lowered by using 1/8 microstepping with a capable stepper driver to rotate the bench. This had great improvements over the previous configuration but also limited the speed to maximum of about 3.5 deg/s. The prototype board was also separated from the rotating bench with dampeners and bubble wrap.

In the gyroscope tests, a flaw in the rotating bench came to light. The screw transmission has an eccentricity and therefore generates systematic error in the measurements. An improved testing bench needs to be built to conduct further testing on the gyroscopes. Due to this, rotating was only limited to around z-axis and no tests around x- and y-axes were made.

As the final result, chosen sensors were BMG160 gyroscope and LIS3MDL magnetometer. The accelerometer is still undecided due to unknown requirements. The required scripts for calibration are made and will be added to the ESTCube knowledge database.

Acknowledgements

I would like to thank my supervisors, Andris Slavinskis and Hendrik Ehrpais, for guiding me throughout my thesis and for leading the ESTCube project. Many thanks to Indrek Sünter, for introducing the logic analyzer and thermal chamber to me, Erik Ilbis, for sharing ideas for the rotating bench improvements, Viljo Allik, for building the existing rotating bench and sharing ideas on improvements, Tarvi Verro, for helping me C, and all members of ESTCube-2 team, who I had various thoughtful discussions with.

Special thanks to all friends and family, who supported me throughout this grand journey.

Madis Kaspar Nigol

Bibliography

[1] Pekka Janhunen. Electrostatic plasma brake for deorbiting a satellite. *J. Propul. Power*, 26:370–372, 2010.

[2] Fatima Ahmed Mohamed and Noor Azian Mohamad Ali. Space debris low earth orbit (leo). *International Journal of Science and Research*, 4(1), January 2015.

[3] A. Slavinskis, M. Pajusalu, H. Kuuste, E. Ilbis, T. Eenmäe, I. Sünter, K. Laizans, H. Ehrpais, P. Liias, E. Kulu, J. Viru, J. Kalde, U. Kvell, J. Kütt, K. Zalite, K. Kahn, S. Lätt, J. Envall, P. Toivonen, J. Polkko, P. Janhunen, R. Rosta, T. Kalvas, R. Vendt, V. Allik, and M. Noorma. Estcube-1 in-orbit experience and lessons learned. In *Aerospace and Electronic Systems Magazine, IEEE*, pages 12–22, 2015.

[4] A. Kestil, T. Tikka, , P. Peitso, J. Rantanen, A. Näsilä, K. Nordling, H. Saari, R. Vainio, P. Janhunen, J. Praks, and M. Hallikainen. Aalto-1 nanosatellite — technical description and mission objectives. *Geosci. Instrum. Method. Data Syst.*, 2:121–130, 2013.

[5] Hendrik Ehrpais, Indrek Sünter, Erik Ilbis, Janis Dalbins, Iaroslav Iakubivsky, Erik Kulu, Indrek Ploom, Pekka Janhunen, Joel Kuusk, Jānis Šate, Roberts Trops, and Andris Slavinskis. Estcube-2 mission and satellite design. In *Small Satellites Systems and Services Symposium*, 2016.

[6] Iaroslav Iakubivskyi, Hendrik Ehrpais, Janis Dalbins, Ervin Oro, Erik Kulu, Johan Kütt, Pekka Janhunen, Andris Slavinskis, Erik Ilbis, Indrek Ploom, Indrek Sünter, Maido Merisalu, and Roberts Trops. ESTCube-2 mission analysis: plasma brake experiment for deorbiting. In *International Astronautical Congress*, September 2016.

[7] Hendrik Ehrpais, Johan Kütt, Madis Kaspar Nigol, Aleksander Parelo, Ikechukwu Ofodile, Karl Kruuse, Hannes Haljaste, Georgi Olentšenko, Joosep Kivastik, Leo Lobski, Mari Liis Pedak, Jose Angel Gutierrez Ahumada, Kristjan Müürsepp, and Andris Slavinskis. Estcube-2 nanosatellite attitude determination and control system design. In *Recent Advances in Space Technologies 2017*, 2017.

[8] Georgi Olentšenko. Prototype design of estcube-2 attitude and orbit control system. Master's thesis, University of Tartu, 2014.

[9] MEMS & Nanotechnology Exchange. What is mems technology? https://www.mems-exchange.org/MEMS/what-is.html, retrieved on May 12, 2017.

[10] PRIME Faraday Partnership. *An Introduction to MEMS*. Loughborough University, January 2002.

[11] Hamamatsu. *S9226 Product Specification*, June 2014.

[12] Maxim Integrated. *MAX21000 Ultra-Accurate, Low Power, 3-Axis Digital Output Gyroscope*, 2 2013. Rev 1.

[13] BOSCH. *BMG160 Digital, triaxial gyroscope sensor*, May 2014. Rev 1.2.

[14] InvenSense. *MPU-6000/MPU-6050 Product Specification*, August 2013. Rev. 3.4.

[15] STMicroelectronics. *L3GD20H MEMS motion sensor: three-axis digital output gyroscope*, March 2013. Rev. 2.

[16] STMicroelectronics. *LSM303D Ultra-compact high-performance eCompass module: 3D accelerometer and 3D magnetometer*, November 2013. Rev 2.

[17] NXP Semiconductors. *FXOS8700CQ 6-axis sensor with integrated linear accelerometer and magnetometer*, March 2016. Rev. 7.0.

[18] STMicroelectronics. *LIS3MDL Digital output magnetic sensor: ultra-low-power, high-performance 3-axis magnetometer*, May 2015. Rev. 4.

[19] Harvey Weinberg. *Gyro Mechanical Performance: The Most Important Parameter*, September 2011.

[20] Brian Schmalz. *Easy Driver Stepper Motor Driver*. Schmalz Haus. http://www.schmalzhaus.com/EasyDriver/.

[21] Stanford Research Systems. *Calibrate Steinhart-Hart Coefficients for Thermistors*, October 2012. Rev B.

Appendix A

Accelerometer thermal chamber tests

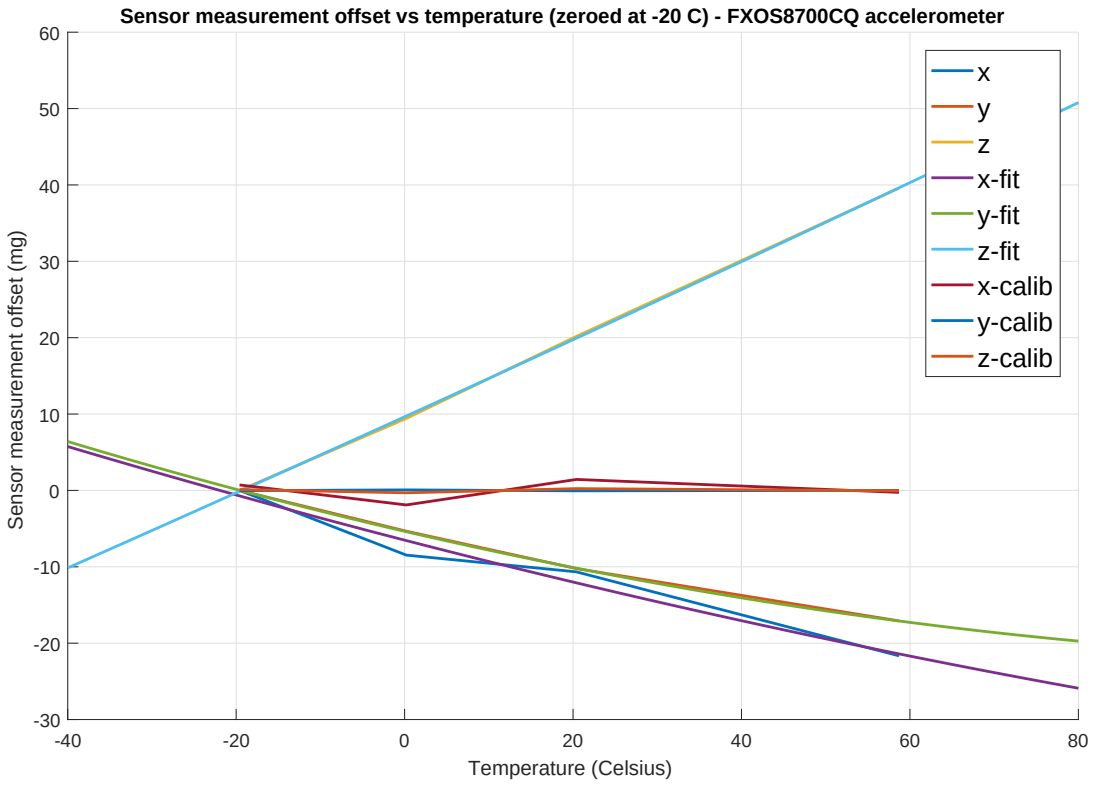

Figure A.1: FXOS8700CQ accelerometer thermal chamber test, fitting functions and corrected data.

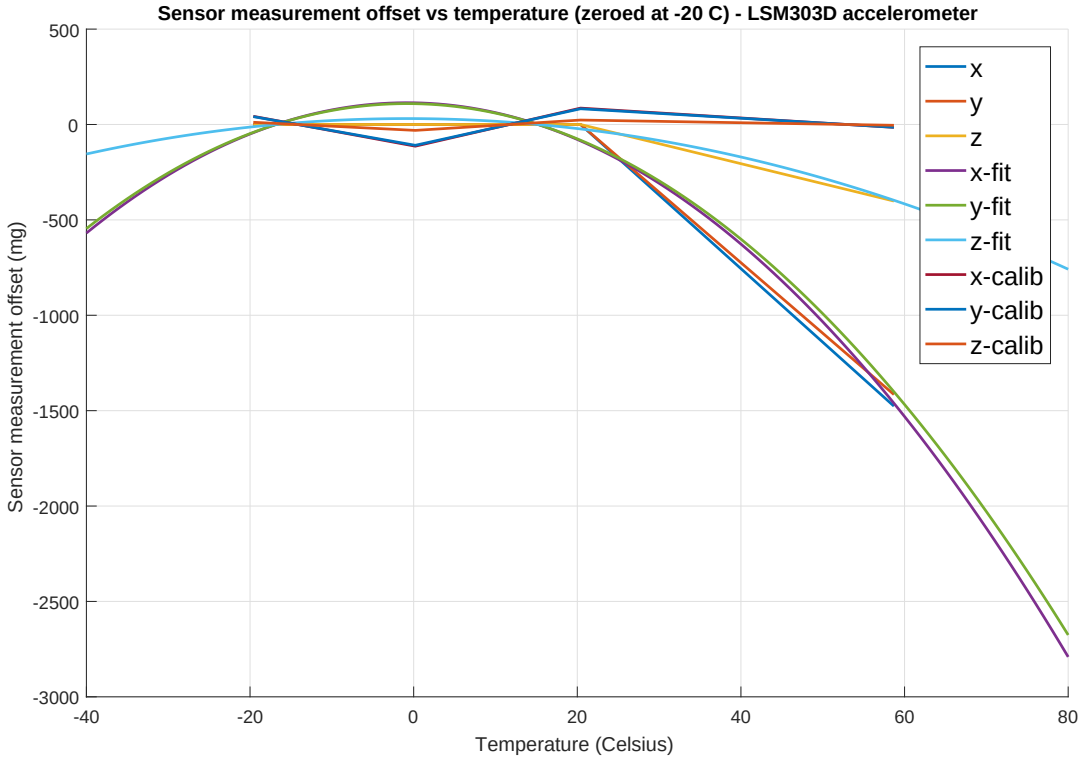

Figure A.2: LSM303D accelerometer thermal chamber test, fitting functions and corrected data.

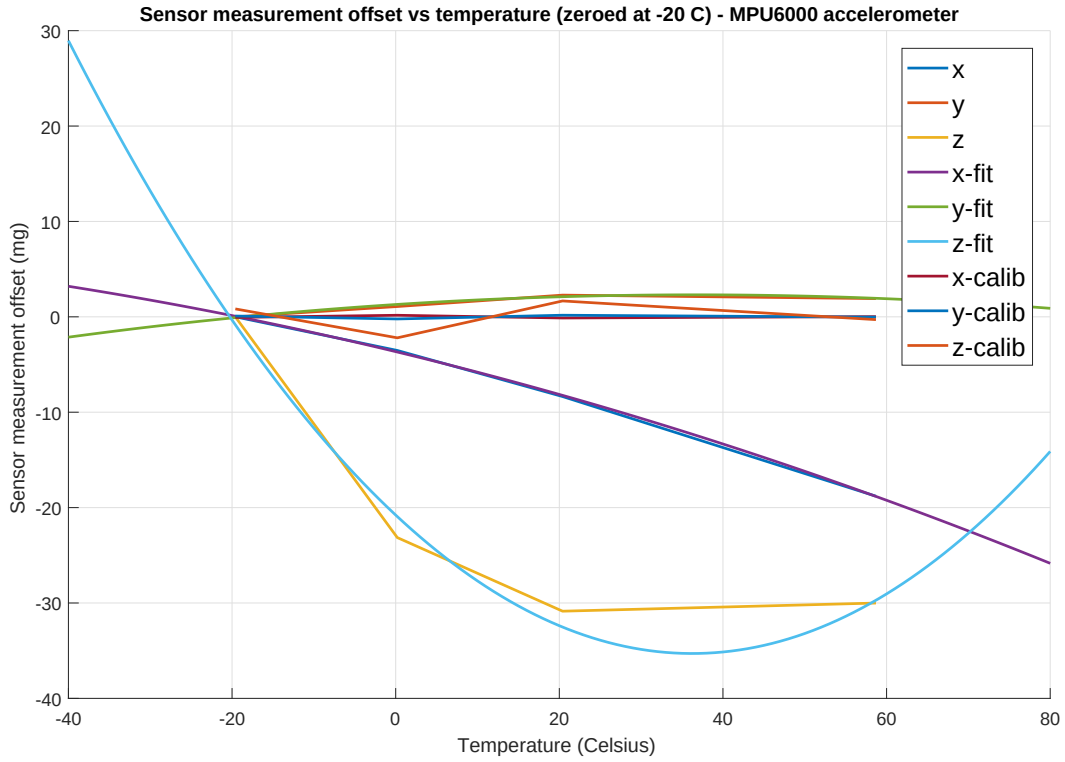

Figure A.3: MPU-6000 accelerometer thermal chamber test, fitting functions and corrected data.

Appendix B

Magnetometer thermal chamber tests

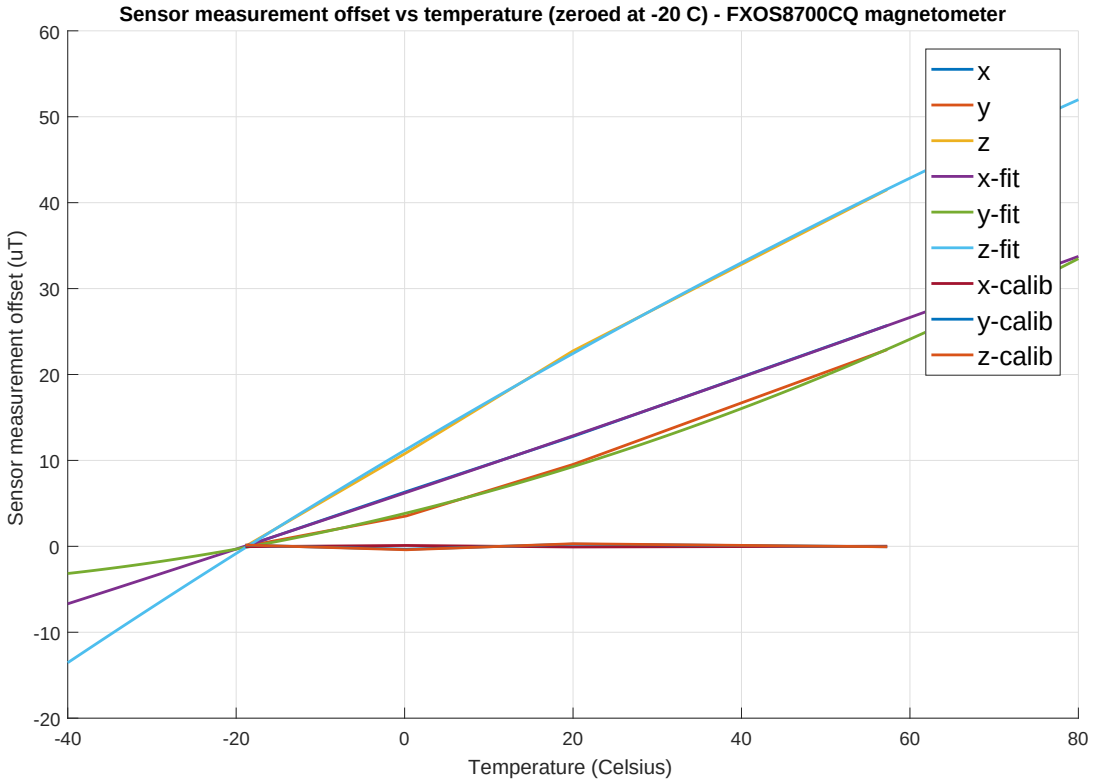

Figure B.1: FXOS8700CQ magnetometer thermal chamber test, fitting functions and corrected data.

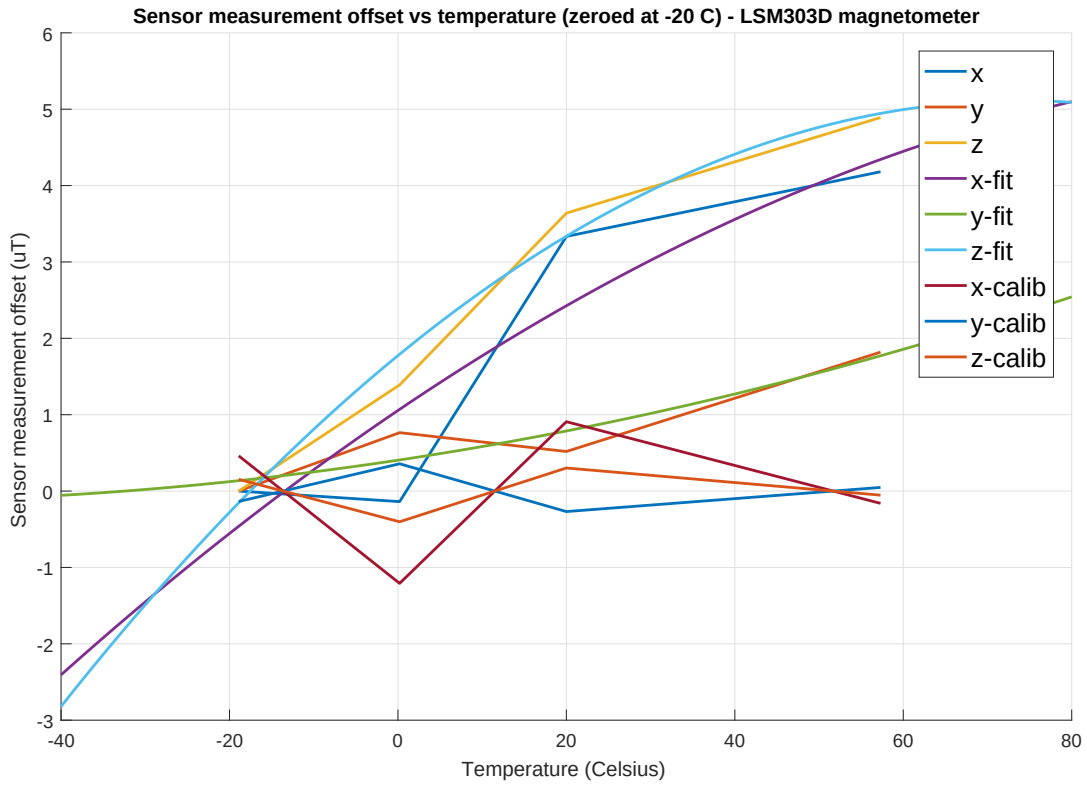

Figure B.2: LSM303D magnetometer thermal chamber test, fitting functions and corrected data.

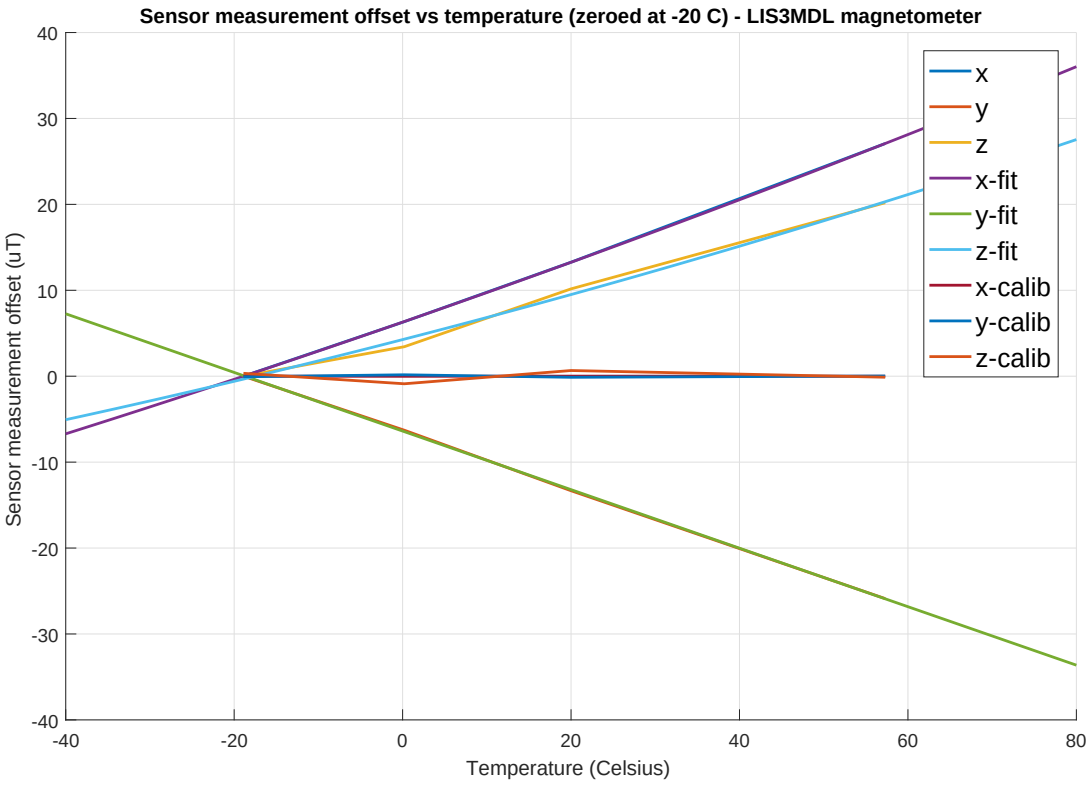

Figure B.3: LIS3MDL magnetometer thermal chamber test, fitting functions and corrected data.

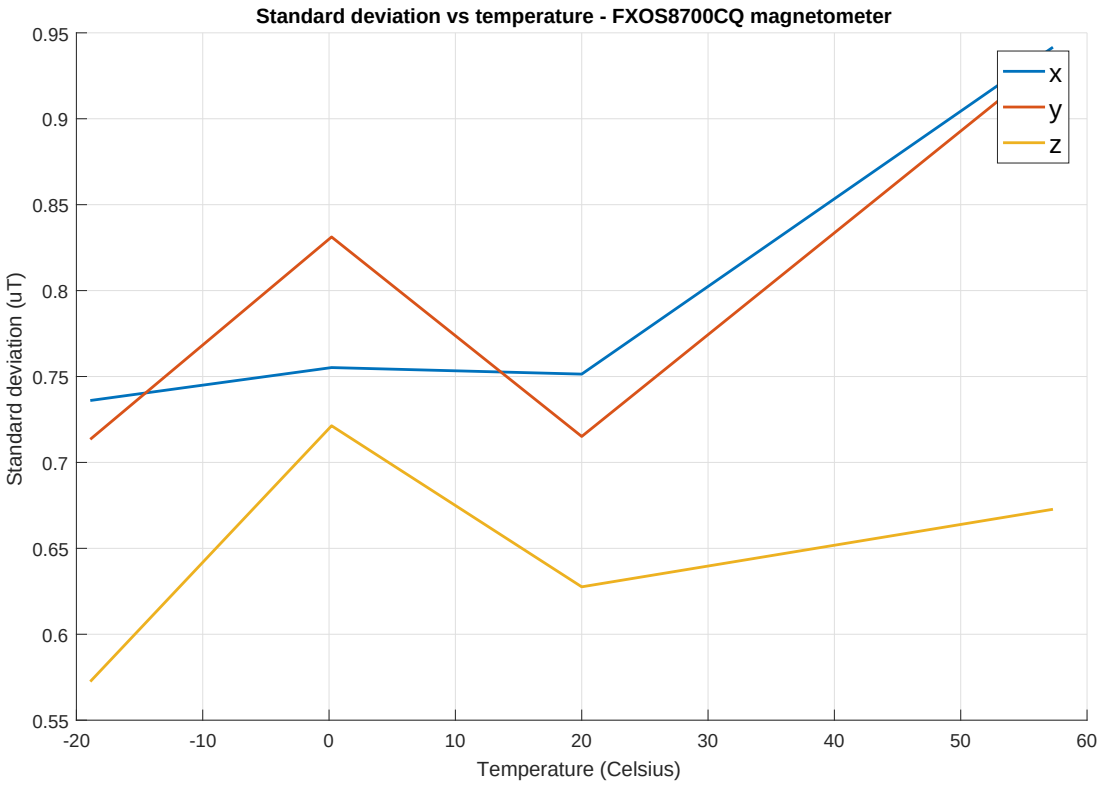

Figure B.4: FXOS8700CQ magnetometer standard deviation vs temperature.

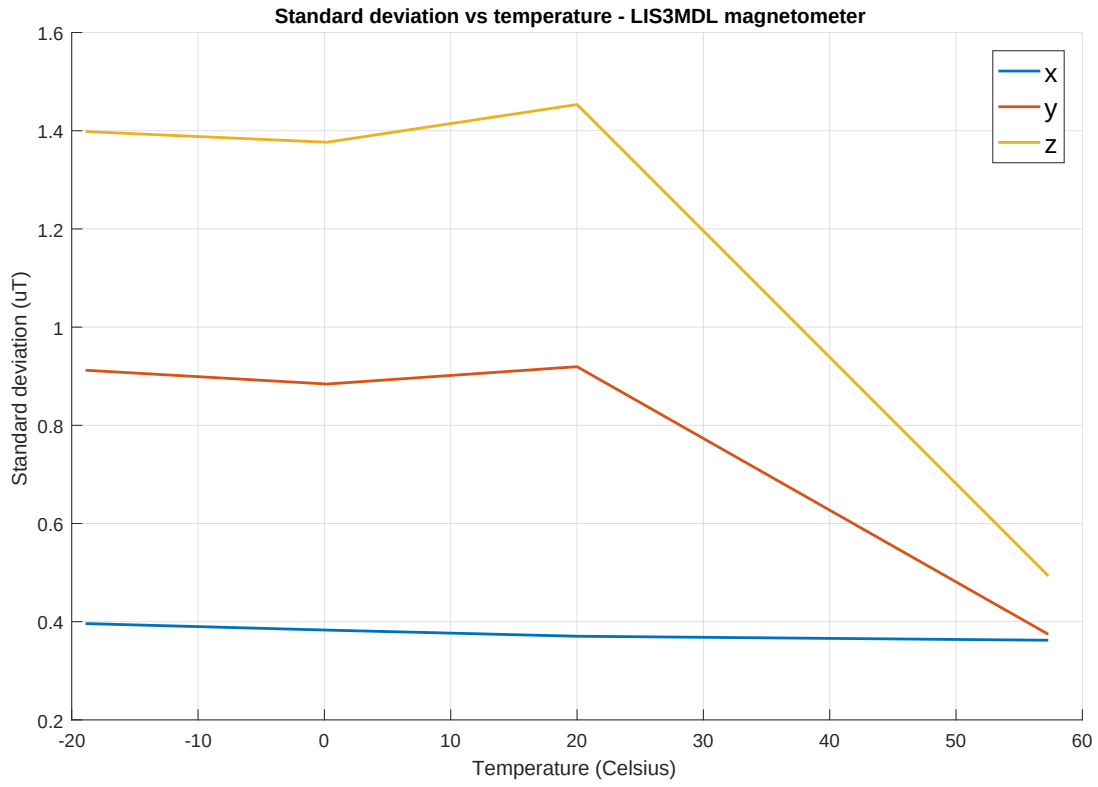

Figure B.5: LIS3MDL magnetometer standard deviation vs temperature.

Lihtlitsents lõputöö reprodutseerimiseks ja lõputöö üldsusele kättesaadavaks tegemiseks

Mina, Madis Kaspar Nigol,

1. annan Tartu Ülikoolile tasuta loa (lihtlitsentsi) enda loodud teose

   ESTCube-2 Attitude and Orbit Control System Sensor Selection and Temperature Calibration,

   mille juhendajad on Dr. Andris Slavinskis ja Hendrik Ehrpais,

   (a) reprodutseerimiseks säilitamise ja üldsusele kättesaadavaks tegemise eesmärgil, sealhulgas digitaalarhiivi DSpace'is lisamise eesmärgil kuni autoriõiguse kehtivuse tähtaja lõppemiseni;

   (b) üldsusele kättesaadavaks tegemiseks Tartu Ülikooli veebikeskkonna kaudu, sealhulgas digitaalarhiivi DSpace'i kaudu kuni autoriõiguse kehtivuse tähtaja lõppemiseni.

2. olen teadlik, et punktis 1 nimetatud õigused jäävad alles ka autorile.

3. kinnitan, et lihtlitsentsi andmisega ei rikuta teiste isikute intellektuaalomandi ega isikuandmete kaitse seadusest tulenevaid õigusi.

Tartu, 25. mai 2017. a.